



ELSEVIER

Contents lists available at ScienceDirect

Physics of the Earth and Planetary Interiors

journal homepage: www.elsevier.com/locate/pepiHPSTAR
049_2014

Compressibility of liquid FeS measured using X-ray radiograph imaging

Jiuhua Chen^{a,b,c,*}, Tony Yu^{c,d}, Shu Huang^a, Jennifer Girard^{a,e}, Xiaoyang Liu^b^a Center for the Study of Matters at Extreme Conditions and Department of Mechanical and Materials Engineering, Florida International University, Miami, FL 33199, USA^b Center for the High Pressure Science and Technology Advanced Research, Jilin University, Changchun 130021, China^c Mineral Physics Institute and Department of Geosciences, Stony Brook University, Stony Brook, NY 11794-2100, USA^d Center for Advanced Radiation Sources, The University of Chicago, Chicago, IL 60637, USA^e Department of Geology and Geophysics, Yale University, New Haven, CT 06511, USA

ARTICLE INFO

Article history:

Available online 2 January 2014

Edited by M. Jellinek

Keywords:

Liquid density

High pressure

Equation of state

Fe–S alloy

X-ray radiograph

Exponential relation of bulk modulus

ABSTRACT

Density of liquid FeS was measured at 1650 K and pressures up to 5.6 GPa using the X-ray absorption radiograph system of the X17B2 beamline at the National Synchrotron Light Source at the Brookhaven National Laboratory. The experimental data were fitted to the third-order Birch–Murnaghan equation of state to calculate the isothermal bulk modulus (K_0) of the liquid, yielding $K_0 = 11 \pm 3$ GPa when the pressure derivative of bulk modulus is fixed at 5. Combining this result with those from previous studies on Fe–S liquid system, we suggest an exponential relation between the liquid Fe–S alloy bulk modulus and its sulfur content.

Published by Elsevier B.V.

1. Introduction

Studies of meteorite composition reveal that iron makes up bulk of the Earth's core. However, seismic observations and mineral physics experimental data indicate that the density of the outer core is about 6–10% less than that of pure Fe at the outer core's pressure and temperature conditions (Birch, 1952; Brett, 1984; Jeanloz, 1979; McQueen and Marsh, 1966). The uncertainties in the density deficit are mainly caused by the uncertainties in the estimated core temperature, and also due to the limited experimental studies on the equation of state (EOS) of liquid iron and its alloys at high temperatures (Li and Fei, 2003). From the mineral physics point of view, properties of light element–iron alloy are critical for determining the candidate element in the core to account for the density deficit. The density deficit indicates that a significant amount of a light element or a combination of several light elements must exist in the outer core as suggested by Birch (1964). A number of light elements, including C, H, O, S, and Si, have been proposed as candidates to present in the core accounting for the density deficit (Hillgren et al., 2000; Poirier, 1994; Stevenson, 1981). Among these elements, sulfur has been widely considered as a strong candidate since it is depleted in the Earth's mantle, easily alloys with iron, and is moderately siderophile during

iron–silicate interaction at high pressures (Kargel and Lewis, 1993; Mason, 1966; Morgan and Anders, 1980; Rama Murthy and Hall, 1970; Sherman, 1997; Usselman, 1975).

Ahrens (Ahrens, 1979) studied density of natural Fe–S materials using shockwave technique and suggested that the amount of sulfur in the core is about 9–12 wt.%. Brown et al. (1984), and Ahrens and Jeanloz (1987) also used shockwave to study the equation of state of FeS at high pressures and high temperatures, and proposed that the amount of sulfur in the core reaches 10 and 11 wt.%, respectively. However, the uncertainty in the equation of state from shockwave data and the differences between solid and liquid phases limit the accuracy of the composition modeling.

Direct measurements of liquid Fe–S density at high pressure became possible about a decade ago. Sanloup et al. (2000) reported density measurements of liquid phase Fe–S alloys using X-ray absorption and large volume high pressure apparatus at the European Synchrotron Radiation Facility (ESRF). They measured the density of Fe–10 wt.%S, Fe–20 wt.%S, and Fe–27 wt.%S within the pressure range of 1.5–6.2 GPa, and derived average isothermal bulk moduli ($K_{0,T}$) of 45 GPa (within 1650–1780 K temperature interval), 30 GPa (within 1600–1700 K temperature interval), and 12 GPa (within 1500–1530 K temperature interval) based on the third-order Birch–Murnaghan equation of state (EOS) for these compositions respectively. Balog and Secco (Balog and Secco, 2003) measured the density of liquid Fe–10 wt.%S alloys using sink–float technique in a large volume press, and reported $K_{0,T} = 63$ GPa at temperatures ranging from 1773 to 2123 K for

* Corresponding author at: Center for the Study of Matters at Extreme Conditions and Department of Mechanical and Materials Engineering, Florida International University, Miami, FL 33199, USA. Tel.: +1 305 348 3140.

E-mail address: chenj@fiu.edu (J. Chen).

the third-order Birch–Murnaghan EOS. The $K_{0,T}$ at different temperatures for Fe–10 wt.%S reported in these two studies (i.e. 45 GPa at 1650–1780 K and 63 GPa at 1773–2123 K) yield a positive $dK_{0,T}/dT$, contradicting to those for common materials. More recently, Nishida et al. (2011) measured densities of liquid FeS in the pressure range up to 3.8 GPa, and reported $K_{0,T} = 2.5$ GPa at $T = 1500$ K. Here we report a result of density measurement of liquid FeS at high pressures up to 5.6 GPa, using the X-ray radiograph system installed at the National Synchrotron Light Source (NSLS) at Brookhaven National Laboratory (BNL).

2. Experimental method

The radiograph system at Beamline X17B2 of NSLS (Chen et al., 2005) includes a YAG crystal as a fluorescent screen, an optical mirror, focusing-magnification lenses, and a CCD camera (Fig. 1). The imaging system is coupled with the cubic-type multi-anvil press SAM85 and interchangeable energy/angle dispersive diffraction systems (Chen et al., 1999). During this study, X-ray diffraction was used for sample identification and pressure determination; X-ray radiograph imaging was used for sample density measurement. A monochromatic X-ray beam was used for the radiograph imaging in order to correlate the image brightness to the sample absorption. The monochromatic beam penetrates through the sample cell and impinges on the fluorescent screen, where a visible sample image based on the intensity of the transmitted X-ray beam is generated. The contrast of the image reflects differences in density, mass absorption, and X-ray path length of the sample and the cell assembly parts.

The X-ray absorption method is applied to this study because of X-ray diffraction method’s incapability for measuring densities of liquid phases. X-ray absorption is governed by the Beer–Lambert law:

$$I = I_0 e^{-\mu \rho d} \quad (1)$$

where I is the intensity of transmitted X-ray beam, I_0 the intensity of incident X-ray beam. The intensity change after the X-ray beam penetrates a homogeneous material is related to the mass absorption coefficient of the material μ (cm^2/g), the density of the material ρ (g/cm^3), and the total travel length of the X-ray beam inside the material d (cm).

Fig. 2 shows the cell assembly of the experiment for liquid density measurements. A boron epoxy cube with 6.15 mm edge length was used as the pressure-transmitting medium. One advantage of using boron epoxy as the pressure medium for holding the sample chamber is its low X-ray absorption, which helps to produce a clear view of the material inside the sample chamber. High temperature was achieved using a cylindrical carbon heater surrounding the sample chamber made of boron nitride. The electric power was introduced through platinum wires and foils which directly bridge

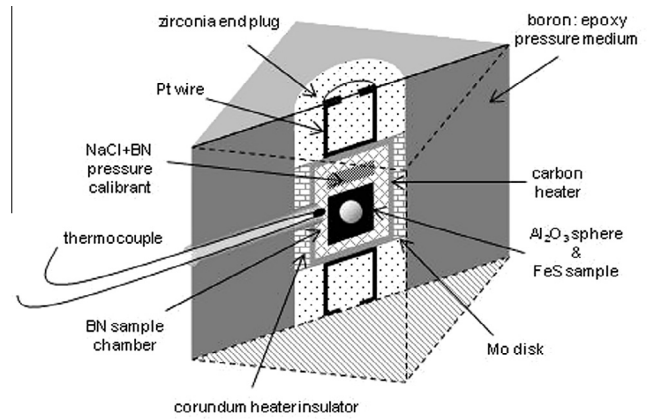


Fig. 2. The cell assembly of the multi-anvil large volume press for liquid density measure using X-ray radiograph.

the tungsten carbide anvil and the heater. The temperature was measured using a W3%Re–W25%Re thermocouple. The thermocouple junction was placed next to the sample chamber. No pressure correction was applied to the W–Re thermocouple emf as such pressure effect is negligible. The experimental uncertainty in sample temperature for this setup is estimated to be 50 K. To measure the density of sample at high pressure and temperature, an Al_2O_3 single crystal reference sphere (0.5 mm in diameter) was embedded in the center of the FeS powder sample. Along with a layer of sodium chloride and boron nitride mixture (as pressure calibrant), the reference sphere and FeS sample were loaded into the sample chamber. The pressure inside the sample chamber during the experiment was inferred by comparing the unit cell volumes of sodium chloride and boron nitride, derived from X-ray diffraction, with their established EOSs.

A monochromatic beam with a cross-section of 2 mm by 2 mm and photon energy of 39.8 keV was used to produce the sample radiograph. As shown in Fig. 3, the brightness $B(x,z)$ on the radiograph image can be presented through a modified Beer–Lambert law equation:

$$B(x,z) = I_0(x,z) K e^{-[\mu_{\text{FeS}} \rho_{\text{FeS}} (D(x,z) - l(x,z)) + \mu_{\text{Al}_2\text{O}_3} \rho_{\text{Al}_2\text{O}_3} l(x,z) + \sum (\mu \rho d)_{\text{surrounding}}]} \quad (2)$$

$$D(x,z) = (D_0^2 - 4x^2)^{\frac{1}{2}} \quad (3)$$

$$l(x,z) = 2 \left[r^2 - (z - z_0)^2 - (x - x_0)^2 \right]^{\frac{1}{2}} \quad (4)$$

where x, y, z represent coordinates with origin on the cylindrical axis of sample chamber; x_0, y_0, z_0 coordinates of the center of the Al_2O_3 sphere; $B(x,z)$ brightness at (x,z) coordinate on the radiograph image; $I_0(x,z)$ incident X-ray intensity at (x,z) coordinate in the beam

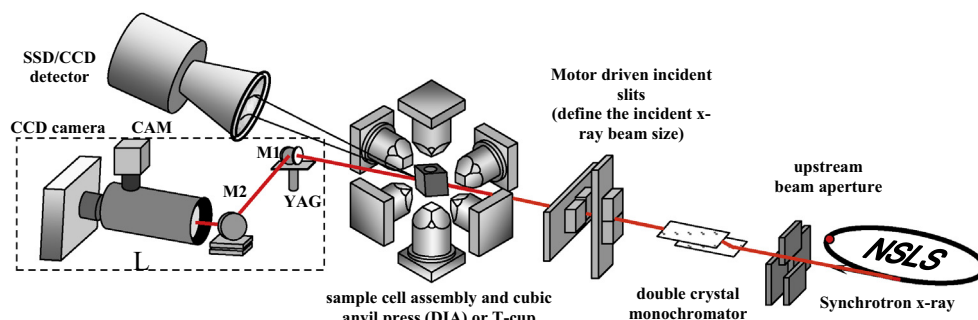


Fig. 1. The radiograph system at Beamline X17B2 of the NSLS.

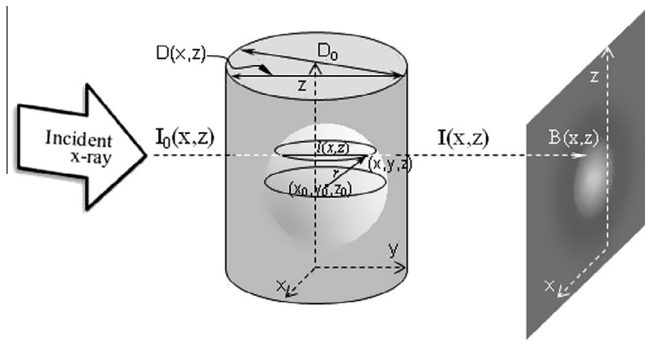


Fig. 3. Schematic of the coordinates for the X-ray radiograph of the reference sphere embedded in the cylindrical sample to derive its density.

cross section; K coefficient of X-ray intensity to radiograph brightness conversion; D_0 the diameter of the cylindrical sample chamber; r the radius of the Al_2O_3 sphere. In the equation, μ_{FeS} , $\mu_{\text{Al}_2\text{O}_3}$ can be calculated from individual atomic mass absorption coefficient (μ_i) and corresponding atomic weight fraction (w_i) in the materials using $\mu = \sum w_i \mu_i$. The μ_{FeS} value is re-evaluated by comparing the derived density with known volume of FeS solid phase before melting. $\rho_{\text{Al}_2\text{O}_3}$ and the sphere radius r at a specific pressure and temperature condition can be calculated from the thermal equation of state of corundum. ρ_{FeS} can then be derived by fitting the brightness data across the whole sphere into the above equation assuming that the absorption of the surrounding materials, such as the pressure medium, sample capsule and heater surrounding the capsule, are uniform across the sample. In a simple case such that only two beams, passing through the reference sphere center and the sample area without the reference sphere respectively, are considered, their corresponding brightness on the radiograph are:

$$B(x_0, 0) = Ce^{-\mu_{\text{FeS}}\rho_{\text{FeS}}(D(x_0, 0))} \quad (5)$$

$$B(x_0, z_0) = Ce^{-[\mu_{\text{FeS}}\rho_{\text{FeS}}(D(x_0, z_0) - r) + \mu_{\text{Al}_2\text{O}_3}\rho_{\text{Al}_2\text{O}_3}r]} \quad (6)$$

Under the assumption of uniformity of the cell, C is a constant and $D(x_0, 0) = D(x_0, z_0)$. Therefore the sample density can be calculated through the following equation without involving the dimension of the sample capsule (D):

$$\rho_{\text{FeS}} = \frac{\mu_{\text{Al}_2\text{O}_3}}{\mu_{\text{FeS}}} \rho_{\text{Al}_2\text{O}_3} + \frac{1}{\mu_{\text{FeS}}r} \ln \frac{B(x_0, z_0)}{B(x_0, 0)} \quad (7)$$

In this method, it is crucial to keep the sample in a cylindrical shape which is sometimes difficult. During our experiments for liquid sample, the deviation of the sample shape from a cylinder is relatively small. Fig. 4 shows an optical image of the cross section along X-ray path in one of the recovered samples. A reasonable uniform shape is preserved. Note the sample may deform more along the direction perpendicular to the X-ray path as a thermocouple is inserted in this direction. In the sample radiograph (Fig. 5a), about 1% distortion across the dimension of the reference

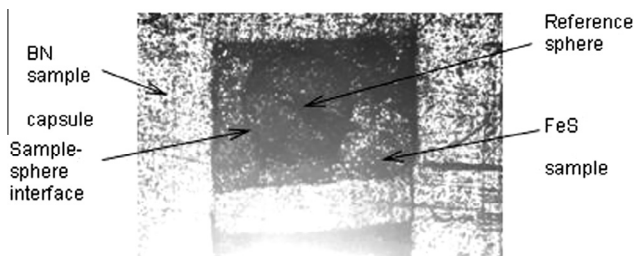


Fig. 4. Optical image of the recovered sample from 5 GPa.

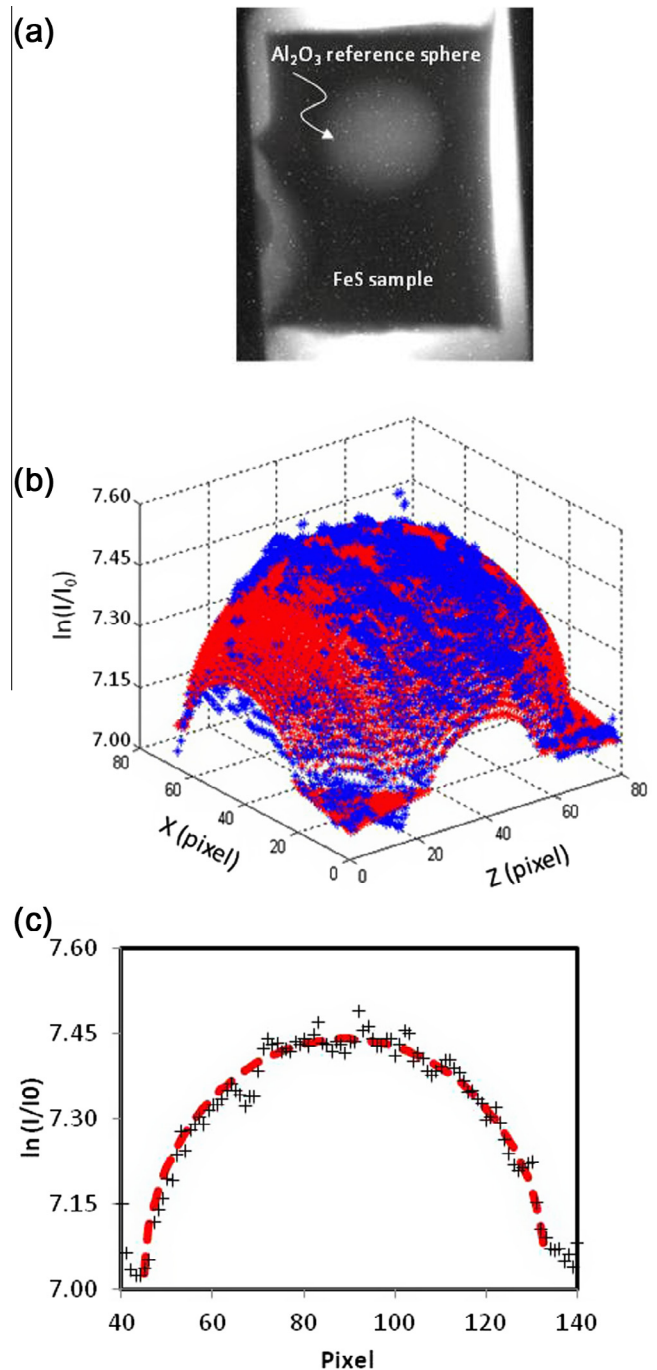


Fig. 5. (a) Radiograph image of the Al_2O_3 sphere in FeS sample at 3.3 GPa; (b) 2-D brightness fitting of the reference sphere. Blue and red symbols are experimental and calculated data, respectively; (c) 1-D brightness fitting across the reference sphere. Crosses and broken line represent the experimental and calculated data respectively. (For interpretation of the references to color in this figure legend, the reader is referred to the web version of this article.)

sphere is observed. However shape of the cross section along X-ray path plays the critical role in the calculation accuracy. During the data processing, two dimensional data across the reference sphere was used to minimize statistic error. The value of D_0 was estimated from the image and fitted as a variable during the data processing.

X-ray diffraction patterns can be collected before and after X-ray radiograph imaging so that changes in cell pressure and sample state (i.e. from solid to liquid) are monitored. Accuracy of the density measurement through the radiograph imaging is estimated

to be 1–2% according to the result of comparative study for measuring density of solid phase using radiograph imaging and X-ray diffraction (Chen et al., 2005).

3. Experimental results

The experiments were performed by applying an initial load to the cell assembly first so that the sample capsule could seal the sample from flowing out when melting occurred. The sample temperature was then increased stepwise to 1650 K. X-ray diffraction patterns of solid sample were taken to derive the solid phase density. This density was used to evaluate the μ_{FeS} value. Assuming the mass absorption coefficients for solid phase and liquid phase are the same, we used derived $\mu_{\text{FeS}} = 0.274 \text{ m}^2/\text{kg}$ for the density calculation of the liquid sample phase. After confirming melting of the sample, X-ray radiograph images of the sample chamber were recorded at five different pressures (3.3, 4.4, 4.5, 4.8 and 5.6 GPa). Fig. 5a shows a radiograph of the sample chamber at 3.3 GPa. The bright circular area on the image results from less X-ray absorption of the corundum reference sphere with regard to the surrounding FeS sample. Main dark area represents the sample owing to its heavy X-ray absorption. The sharp dark edges on both sides of the sample are shadows of WC anvils of the cubic type multi-anvil press. The tip of the thermocouple junction is also shown at the lower left side of the image. A non-linear regression fitting based on Eq. (2) was used in a selected area around the reference sphere for determining the melt density. An example of the fitting result is shown in Fig. 5b. The blue points are the measured data, and the red ones are the calculated data points that best fit the observation. This provides a complete coverage of the fitting area taking account of the whole reference sphere, and therefore generates a more statistically reliable result than any one dimensional analysis across the reference sphere (Fig. 5c).

The experimental results of derived densities are listed in Table 1. These data were fitted into the third-order Birch–Murnaghan EOS (Birch, 1947):

$$P(\rho, T) = 3K_{0,T}f(\rho, T)(1 + 2f(\rho, T))^{5/2} \left(1 + \frac{3}{2}(K'_{0,T} - 4)f(\rho, T) \right) \quad (8)$$

where $f(\rho, T) = [(\rho(T)/\rho_0(T))^{2/3} - 1]/2$, to derive isothermal bulk modulus $K_{0,T}$. The EosFit5.2 program (Angel, 2000) was used for the data processing. Because of the limited pressure range for these data, we had to limit the fitting variables to ambient pressure density, $\rho_0(T)$, and isothermal bulk modulus, $K_{0,T}$, while fix the pressure derivative of the isothermal bulk modulus, $K'_{0,T}$. Sanloup et al. (2000) also fixed $K'_{0,T}$ to derive $K_{0,T}$ from their compression data up to 6 GPa for Fe–Xwt.%S alloys. They used $K'_{0,T} = 4, 5, 6$ and 7 to estimate possible range of the bulk modulus through the third-order Birch–Murnaghan EOS and used the average value to represent $K_{0,T}$. In a later work, Balog and Secco (2003) derived $K'_{0,T} = 4.8$ using their density data of Fe–10 wt.%S up to 20 GPa and the third-order Birch–Murnaghan EOS. We therefore processed our data by fixing $K'_{0,T} = 5.0$, taking into account the $K'_{0,T}$ values from both of these studies. The fitting yields: $\rho_0(1650 \text{ K}) = 4.2 \pm 0.2 \text{ (g/cm}^3\text{)}$, and $K_{0,1650\text{K}} = 11 \pm 3 \text{ GPa}$ for the liquid FeS sample.

The isothermal bulk modulus of FeS liquid derived here is significantly higher than the value ($K_{0,1500\text{K}} = 2.5 \pm 0.3 \text{ GPa}$) recently

reported by Nishida et al. (2011) when they constrained their high pressure data with ambient pressure density (3.67 g/cm^3) calculated from maximum bubble data for liquid $\text{Fe}_{48.7}\text{S}_{51.3}$ at 1500 K (Nagamori, 1969). During their data processing, Nishida et al. (2011) had to use Vinet EOS for deriving the isothermal bulk modulus as the data did not fit Birch–Murnaghan EOS smoothly. They speculated that the cause of this is a discontinuous increase in the density associated with a possible structural change in liquid FeS at a very low pressure (<0.5 GPa) and Vinet EOS is superior to other types of EOS for soft materials, such as liquids (Vinet et al., 1989). We therefore also tried to fit our data into Vinet EOS:

$$P(\rho, T) = 3K_{0,T} \frac{1 - f_V(\rho, T)}{f_V^2(\rho, T)} e^{\frac{3}{2}(K'_{0,T} - 1)(1 - f_V(\rho, T))} \quad (9)$$

where $f_V(\rho, T) = [\rho_0(T)/\rho(T)]^{1/3}$, and obtained $\rho_0(1650 \text{ K}) = 4.2 \pm 0.2 \text{ (g/cm}^3\text{)}$, and $K_{0,1650\text{K}} = 12 \pm 3 \text{ GPa}$. The results of both ambient pressure density, $\rho_0(1650 \text{ K})$, and isothermal bulk modulus, $K_{0,1650\text{K}}$, derived from the third-order Birch–Murnaghan EOS and Vinet EOS for our data are nearly identical within the experimental uncertainty (Table 2). These results actually agree with those by Nishida et al. (2011) extremely well when they ignored the data below 0.5 GPa and fitted only the data at pressures between 2.1 and 3.8 GPa, which yielded: $\rho_0 = 4.23 \pm 0.03 \text{ (g/cm}^3\text{)}$, and $K_0 = 12 \pm 3 \text{ GPa}$. Nevertheless, the pressure derivative of bulk modulus in their result is much higher $K'_0 = 14 \pm 3$, with respect to the value we used, and the temperature of their result is 150 K lower. While our experiments extended the upper pressure range for liquid FeS density data from 3.8 to 5.6 GPa, much more data are needed to understand the compression behavior of this material.

Finally, we tried to combine our data and those from Nishida et al. (2011) since they are collected on the same sample composition using similar techniques, and cover different pressure range (3.3–5.6 and 0.4–3.8 GPa, respectively). Using an average thermal expansion coefficient value $\alpha = 4.8 \times 10^{-4} \text{ K}^{-1}$ calculated from published data (Kaiura and Toguri, 1979; Nagamori, 1969), we normalized the density data from Nishida et al. (2011) at 1500, 1600, 1700 and 1800–1650 K so that they can be combined with current data for isothermal EOS fitting. Both of the data are plotted in Fig. 6. For comparison, data from Sanloup et al. (2000) and Balog and Secco (2003) are also shown in the figure. Fitting the combined data into the third-order Birch–Murnaghan EOS yields $\rho_0(1650 \text{ K}) = 3.8 \pm 0.1 \text{ (g/cm}^3\text{)}$, and $K_{0,1650\text{K}} = 7 \pm 2 \text{ GPa}$ when fixing $K'_{0,T} = 5.0$. Convincingly, fitting these data into Vinet EOS produced nearly identical results. The combined data yield new values beyond the uncertainty range of the results from individual data sets, indicating the pressure range of either individual data set is too narrow with regard to the experimental accuracy. More experimental data with improved accuracy for melt density measurement are highly demanded to produce more robust result. For the same reason, the result from the combined data may reflect more reliable values. The derived density at ambient pressure $\rho_0 = 3.8 \text{ g/cm}^3$ from the combined data is consistent with the result by Kaiura and Toguri (1979) using a bottom-balance Archimedean technique (ca. 3.83 g/cm^3 at 1625 K). Therefore the data can be justified without the structural transition in the melt at pressure below 0.5 GPa (Nishida et al., 2011; Urakawa et al., 1998).

4. Discussion and geophysical implications

Sanloup et al. (2000) investigated their results of isothermal bulk modulus of Fe–S liquid system as a function of S content together with previous data of liquid Fe (Hixson et al., 1990), and concluded that 1 wt.%S approximates a decreases of 2.5 GPa in $K_{0,T}$. Nishida et al. (2011) reported that the $K_{0,T}$ (2.5 GPa) they derived for FeS liquid is close to the extrapolation of the relation be-

Table 1
Densities of FeS liquid at 1650 K obtained through X-ray radiograph.

P (GPa)	3.32	4.40	4.52	4.79	5.62
Error in P (GPa)	0.05	0.05	0.06	0.05	0.07
ρ (g/cm^3)	5.03	5.18	5.20	5.30	5.38
Error in ρ (g/cm^3)	0.08	0.08	0.08	0.11	0.09

Table 2
Experimental results of isothermal bulk modulus and its pressure derivative for Fe–S liquids.

Composition		This study		Nishida et al. (2011)		This study and Nishida et al. (2011)		Balog and Secco (2003)		Sanloup et al. (2000)		
		wt.%	Fe–36 wt.%S	Fe–36 wt.%S	Fe–36 wt.%S	Fe–10 wt.%S	Fe–10 wt.%S	Fe–10 wt.%S	Fe–10 wt.%S	Fe–10 wt.%S	Fe–20 wt.%S	Fe–27 wt.%S
	atm.%	Fe _{0.5} S _{0.5}	Fe _{0.5} S _{0.5}	Fe _{0.84} S _{0.16}	Fe _{0.84} S _{0.16}	Fe _{0.84} S _{0.16}	Fe _{0.7} S _{0.3}	Fe _{0.61} S _{0.39}				
Pressure range (GPa)		3.3–5.6	0–3.8	2.1–3.8	0.4–5.6			1–20		2.1–6.0	2.3–6.2	1.5–4.0
Temperature (K)		1650	1500	1500	1650*			1773–2123		1650–1780	1600–1700	1500–1530
Birch–Murnaghan EOS	$K_{0,T}$ (GPa)	11 ± 3			7 ± 2			63		45 ± 5	30 ± 5	12 ± 6
	K'_0	5 (fixed)			5 (fixed)			4.8		4–7 (fixed)	4–7 (fixed)	4–7 (fixed)
Vinet EOS	$K_{0,T}$ (GPa)	12 ± 3	2.5 ± 0.3	12 ± 3	7 ± 2			60				
	K'_0	5 (fixed)	24 ± 2	14 ± 3	5 (fixed)			4.8				

* Converted to 1650 K using average thermal expansion coefficient value $\alpha = 4.8 \times 10^{-4} \text{ K}^{-1}$ calculated from published data (Nagamori, 1969; Kaiura and Toguri, 1979).

tween $K_{0,T}$ and S content determined by Sanloup et al. (2000). We plot the currently available experimental data of $K_{0,T}$ for liquid Fe–S system in Fig. 7. In addition to the data listed in Table 2, we use $K_{0,T} = 88 \text{ GPa}$ for pure Fe liquid from Nasch and Manghnani (1998) instead of 82 GPa (Hixson et al., 1990) and $K_{0,T} = 1.6 \text{ GPa}$ for pure S liquid from Tsuchiya (Tsuchiya, 1994). The data are plotted against atomic fraction of S. It seems that all the data (excluding pure S liquid) can be approximately fitted into a linear relation yielding a decrease in $K_{0,T}$ by 1.8 GPa every 1 atm%. However, this linear relation leads a negative $K_{0,T}$ when S content increases beyond 50 atm%. This indicates that there is probably a change of compression mechanism in the Fe–S melt system at the composition of about 1:1 M ratio. Because the structure of molten Fe is simple metallic liquid (Alfè et al., 2000) whereas liquid S has circular-molecule structure (Ludwig et al., 2002), such a compression mechanism change is possible. On the other hand, to understand the compositional dependence of $K_{0,T}$, we evaluated upper and lower limits of the $K_{0,T}$ using common rule of mixtures equations used for predicting upper (Voigt) and lower (Reuss) bound of elastic modulus for a composite of A and B:

$$K_{\text{upper}} = K_A V_A + K_B V_B \quad (10)$$

$$K_{\text{lower}} = \frac{K_A K_B}{K_A V_B + K_B V_A} \quad (11)$$

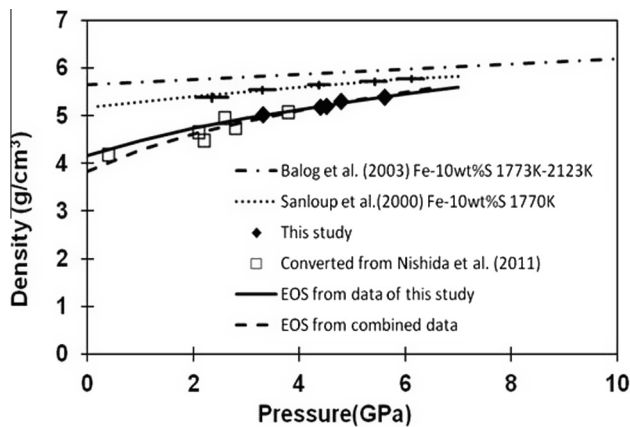


Fig. 6. Experimental data of FeS liquid density as a function of pressure at 1650 K. The data from Nishida et al. (2011) are normalized from different temperatures using a thermal expansion coefficient $\alpha = 4.8 \times 10^{-4} \text{ K}^{-1}$ (see text for details). The combined data include data from this study and those converted from Nishida et al. (2011).

where V_A and V_B are the volume fraction of component A and B respectively. After converting the volume fraction into atomic fraction, the upper and lower limits are plotted in Fig. 7. Most of the experimental data fall within the boundaries, except that the value of $K_{0,T}$ (2.5 GPa) for FeS from Nishida et al. (2011) is below the lower bound. The possible reason for this may be because they used a very low density data at ambient pressure in their EOS fitting. When they used only the data at high pressures ($P > 0.5 \text{ GPa}$), they obtained $K_{0,T} = 12 \pm 3 \text{ GPa}$, which falls within the boundaries. To find a better expression to represent the compositional relation of $K_{0,T}$ for the liquid Fe–S system, we start with an exponential function $K = C_0 \exp(C_1 w)$, C_0 , C_1 : constant; w atomic fraction, and derive a relation:

$$K_{\text{Fe-S}} = K_{\text{Fe}} e^{-w_S \ln(K_{\text{Fe}}/K_S)} \quad (12)$$

or

$$K_{\text{Fe-S}} = (K_{\text{Fe}})^{w_{\text{Fe}}} (K_S)^{w_S} \quad (13)$$

where K_{Fe} and K_S are bulk moduli of liquid Fe and S end members respectively, and w_{Fe} , w_S are the atomic fraction of Fe and S respec-

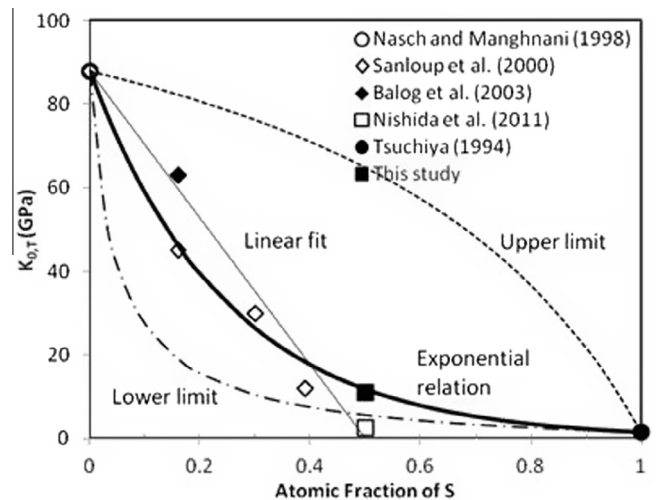


Fig. 7. Isothermal bulk modulus ($K_{0,T}$) of Fe–S liquid system as a function of sulfur content. Broken line indicates the upper limit of $K_{0,T}$ predicted by volume-fraction weighted average of two end members; dashed-dotted line indicates the lower limit estimated through volume fraction weighted reciprocal sum of two end members; hair line represents the linear fit to all experimental data excluding pure S; and the bold line represents predicted $K_{0,T}$ by the exponential relation (see text for details).

tively. As shown in Fig. 7, this relation (bold line) may represent the bulk modulus throughout the entire composition range between the two end members. It is noted that no temperature corrections are made when we plot the $K_{0,T}$ of Table 2 in Fig. 7, for two reasons: (a) some $K_{0,T}$ values are derived from a temperature interval not at a constant T ; (b) such correction makes only a difference of 2–3 GPa since dK/dT is in the order of -10^{-2} to -10^{-3} GPa/K (Nishida et al., 2011). In addition, there is a discrepancy between the data from Sanloup et al. (2000) and Balog and Secco (2003) at 16 atm% S if consider the temperature effect on bulk modulus: 45 GPa at 1770 K from the former and 63 GPa at 1773–2123 K from the latter yield a positive dK/dT . This is opposite to common temperature effect on bulk modulus. The techniques used in these two studies are very different. Balog and Secco (2003) used sphere sink/float technique to bracket the sample density while Sanloup et al. (2000) used X-ray absorption to determine the density. If using exponential relation to evaluate the data, the result from Sanloup et al. (2000) based on a technique similar to that used in this study is closer to the model, whereas the result from Balog and Secco (2003) fit into the linear relation better.

The exponential relation and the linear relation (i.e. the bold line and hair line in Fig. 7) predict same $K_{0,T}$ value at 40 atm% S content. However, at the possible liquid outer core composition, 10 wt.% S (or ~ 16 atm% S), the two relations present a 14 GPa difference in $K_{0,T}$ (60 GPa from the linear relation and 46 GPa from the exponential relation). Although it is impossible to extrapolate the current EOS obtained at very limited pressure range to the conditions of Earth's outer core, this difference in $K_{0,T}$ resulted from the different compositional relations will be carried to the core conditions when identical pressure and temperature derivatives are used for both cases. Considering that 1 atm% change in composition causes 1.8 GPa change in $K_{0,T}$, this difference of 14 GPa in $K_{0,T}$ represents nearly 8 atm% deviation, which is equivalent to about 5 wt.% change at the composition around 10 wt.%. Therefore, much more accurate density data of Fe–S liquid system in an extended pressure range are needed to supply a meaningful constrain on the core composition in terms of sulfur content to account for the density deficit of the liquid outer core.

Acknowledgements

This research was conducted at the beamline partially supported by COMPRES, under NSF Cooperative Agreement EAR 06-49658. We would like to thank Dr. Michael T. Vaughan, Dr. Liping Wang, Dr. Hongbo Long and Dr. Donald J. Weidner for their technical support at the beamline and insightful discussions. Use of the NSLS, Brookhaven National Laboratory, was supported by the U.S. Department of Energy, under Contract No. DE-AC02-98CH10886. The research was supported by NSF (Award EAR-0711321 and EAR-1015509). A part of the data analysis was performed during the summer when J.C. was supported partially by DOE (Grant No. DE-FG02-07ER46461) and by the EFree, an Energy Frontier Research Center funded by the U.S. Department of Energy, Office of Science, Office of Basic Energy Sciences under Award Number DE-SC0001057. We would like to thank Dr. Yingwei Fei and other two anonymous reviewers for their supportive review and suggestive comments to improve the quality of the paper.

References

Ahrens, T.J., 1979. Equations of state of iron sulfide and constraints on the sulfur content of the Earth. *J. Geophys. Res.* 84, 985–998.

- Ahrens, T.J., Jeanloz, R., 1987. Pyrite shock compression, isentropic release and composition of the Earth's core. *J. Geophys. Res.* 92, 10,363–310,375.
- Alfe, D., Kresse, G., Gillan, M.J., 2000. Structure and dynamics of liquid iron under Earth's core conditions. *Phys. Rev. B*, <http://dx.doi.org/10.1103/physrevb.1161.1132>.
- Angel, R., 2000. Equations of state. In: Hazen, R.M., Downs, R.T. (Eds.), *High-Pressure, High-Temperature Crystal Chemistry*. MSA, pp. 35–60.
- Balog, P.S., Secco, R.A., 2003. Equation of state of liquid Fe–10 wt% S: implications for the metallic cores of planetary bodies. *J. Geophys. Res.* 108, 2124, <http://dx.doi.org/10.1029/2001JB001646>.
- Birch, F., 1947. Finite elastic strain of cubic crystals. *Phys. Rev.* 71, 809–824.
- Birch, F., 1952. Elasticity and constitution of the Earth's interior. *J. Geophys. Res.* 57, 227–286.
- Birch, F., 1964. Density and composition of mantle and core. *J. Geophys. Res.* 69 (20), 4377–4388.
- Brett, R., 1984. Chemical equilibrium of the Earth's core and upper mantle. *Geochem. Cosmochim. Acta* 48, 1183–1188.
- Brown, J.M., Ahrens, T.J., Shampine, D.L., 1984. Hugoniot data for pyrrhotite and the Earth's core. *J. Geophys. Res.* 89, 6041–6048.
- Chen, J., Weidner, D.J., Vaughan, M.T., Parise, J.B., Zhang, J., Xu, Y., 1999. A combined CCD/IP detection system for monochromatic XRD studies at high pressure and temperature. In: Manghnani, M.H., Nellis, W.J., Nicol, M.F. (Eds.), *Science and Technology of High Pressure*. Universities Press Ltd, Hyderabad, pp. 1035–1038.
- Chen, J., Weidner, D.J., Wang, L., Vaughan, M.T., Young, C.E., 2005. Density measurements of molten materials at high pressure using synchrotron x-ray radiography: melting volume of FeS. In: Chen, J., Wang, Y., Duffy, T.S., Shen, G., Dobrzynetskiy, L.F. (Eds.), *Advances in High-Pressure Technology for Geophysical Applications*. Elsevier, Amsterdam, pp. 185–194.
- Hillgren, V.J., Gessmann, C.K., Li, J., 2000. An experimental perspective on the light element in Earth's core. In: Canup, R.M., Righter, K. (Eds.), *Origin of the Earth and Moon*. The University of Arizona Press, Tucson, pp. 245–263.
- Hixson, R.S., Winkler, M.A., Hodgdon, M.L., 1990. Sound speed and thermophysical properties of liquid-iron and nickel. *Phys. Rev. B* 42, 6485–6491.
- Jeanloz, R., 1979. Properties of iron at high pressures and the state of the core. *J. Geophys. Res.* 84, 6059–6069.
- Kaiura, G.H., Toguri, J.M., 1979. Densities of the molten FeS, FeS–Cu2S and Fe–S–O systems – utilizing a bottom-balance archimedean technique. *Can. Metall. Q.* 18, 155–164.
- Kargel, J.S., Lewis, J.S., 1993. The composition and early evolution of Earth. *Icarus* 105, 1–25.
- Li, J., Fei, Y., 2003. Experimental constraints on core composition. In: Carlson, R.W. (Ed.), *Geochemistry of the Mantle and Core*. Elsevier, pp. 521–546.
- Ludwig, R., Behler, J., Klöck, B., Weinhold, F., 2002. Molecular composition of liquid sulfur. *Angew. Chem. Int. Ed.* 41, 3199–3202.
- Mason, B., 1966. Composition of the Earth. *Nature* 211, 616–618.
- McQueen, R.G., Marsh, S.P., 1966. Shock-wave compression of iron-nickel alloys and the Earth's core. *J. Geophys. Res.* 71, 1751–1756.
- Morgan, J.W., Anders, E., 1980. Chemical composition of Earth, Venus, and Mercury. *Proc. Natl. Acad. Sci. U.S.A.* 77, 6973–6977.
- Nagamori, M., 1969. Density of molten Ag–S, Au–S, Fe–S, and Ni–S systems. *Trans. Metall. Soc. AIME* 245, 1897.
- Nasch, P.M., Manghnani, M.H., 1998. Molar volume, thermal expansion, and bulk modulus in liquid Fe–Ni alloys at 1 bar: evidence for magnetic anomalies? In: Manghnani, M.H., Yagi, T. (Eds.), *Properties of Earth and Planetary Materials at High Pressure and Temperature*, Geophysical Monograph 101. American Geophysical Union, Washington, D.C., pp. 307–317.
- Nishida, K., Ohtani, E., Urakawa, S., Suzuki, A., Sakamaki, T., Terasaki, H., Katayama, Y., 2011. Density measurement of liquid FeS at high pressures using synchrotron X-ray absorption. *Am. Mineral.* 96, 864–868.
- Poirier, J.P., 1994. Light elements in the Earth's outer core: a critical review. *Phys. Earth Planet. Int.* 85, 319–337.
- Rama Murthy, V., Hall, H.T., 1970. The chemical composition of the Earth's core: possibility of sulfur in the core. *Phys. Earth Planet. Int.* 2, 276–282.
- Sanloup, C., Guyot, F., Gillet, P., Fiquet, G., Mezouar, M., Martinez, I., 2000. Density measurements of liquid Fe–S alloys at high pressure. *Geophys. Res. Lett.* 27, 811–814.
- Sherman, D.M., 1997. The composition of the Earth's core: constraints on S and Si vs. temperature. *Earth Planet. Sci. Lett.* 153, 149–155.
- Stevenson, D.J., 1981. Models of the Earth's core. *Science* 214, 611–619.
- Tsuchiya, Y., 1994. The thermodynamics of structural-changes in the liquid sulfur tellurium system – compressibility and ehrenfest relations. *J. Phys.-Condens. Matter* 6, 2451–2458.
- Urakawa, S., Igawa, N., Kusaba, K., Ohno, H., Shimomura, O., 1998. Structure of molten iron sulfide under high pressure. *Rev. High Press. Sci. Technol.* 7, 286–288.
- Usselman, T.M., 1975. Experimental approach to the state of the core, part I, the liquidus relation of the Fe-rich portion of the Fe–Ni–S system at 30 to 100 kbar and part II, composition and thermal regime. *Am. J. Sci.* 275 (278–290), 291–303.
- Vinet, P., Rose, J.H., Ferrante, J., Smith, J.R., 1989. Universal features of the equation of state of solids. *J. Phys.-Condens. Matter* 1, 1941–1963.